

Numerical experimentation of a diagnostic model of 3-D circulation in the Arabian Sea

C Shaji, N Bahulayan*, S K Dube & A D Rao

Centre for Atmospheric Sciences, Indian Institute of Technology, New Delhi 110016, India

*Physical Oceanography Division, National Institute of Oceanography, Goa 403004, India

Received 15 October 1996, revised 10 February 1997

Climatic circulation in the upper levels of the Arabian Sea and western equatorial Indian Ocean are computed using a 3-dimensional, 33 level diagnostic circulation model. A steady state solution is obtained within 30 days of model integration. Model has been successful in computing all the major current systems in the Arabian Sea and western equatorial Indian Ocean during NE and premonsoon seasons. Computed currents are compared with available observations on currents at selected regions in the model area and it has been found that both agreed fairly well. Model results are also explained in terms of the forcing parameters and the dynamics considered in the model.

Local forcings of wind and vertical density variation play a significant role in driving the 3-D circulation in the ocean. The observed circulation is mainly the resultant of wind-driven and thermohaline components. Diagnostic modelling approach is one of the techniques normally used to study the 3-D circulation in the ocean, in which wind field, thermohaline field and bottom relief of the ocean is considered as the main forcings. Equation of state used in diagnostic model is only to compute the density field and the density is kept constant throughout the model integration. A closed system of diagnostic model equations will consist, in addition to hydrodynamical equations, a derived relation for integral function either in terms of mass transport stream function or sea surface topography. One advantage of the diagnostic model is that it takes only a small fraction of the computer time required for prognostic ocean circulation models. In the present paper, a 3-dimensional, 33 level diagnostic circulation model has been used to compute the climatological circulation in the Arabian Sea and western equatorial Indian Ocean. Model is forced by climatologically averaged seasonal winds and thermohaline field at different levels. In the following sections, diagnostic model equations, its boundary and initial conditions, numerical solution procedure, results of computation for the winter

(NE monsoon) and spring (premonsoon) seasons are presented.

Materials and Methods

Model equations

For the present model, the basic hydrodynamical equations governing the large scale 3-dimensional flows in spherical co-ordinate system were taken from Gill¹. The model has been described in detail by Bahulayan & Shaji². A brief description of the characteristics of the model is presented here.

Scale analysis of the governing equations shows that non-linear and friction terms have the same order of magnitude and both play a major role in the dynamics of circulation in the equatorial regions where geostrophy fails. The sign convention used in this model is different from the standard sign convention used in oceanography. A co-ordinate system wherein the longitude(λ), the co-latitude(θ) and vertical co-ordinate(z) increase towards east, south and downward directions respectively is adapted in the present model. After considering the approximations of Boussinesq, hydrostatics and incompressibility, the final model equations can be written as follows.

$$\frac{\partial u}{\partial t} + Au + Iv + \cot \theta \frac{uv}{R} = -\frac{1}{\rho_0 R \sin \theta} \frac{\partial p}{\partial \lambda} + F^\lambda \dots (1)$$

$$\frac{\partial v}{\partial t} + Av - lu - \cot \theta \frac{u^2}{R} = -\frac{l}{\rho_o R} \frac{\partial p}{\partial \theta} + F^\theta \dots (2)$$

$$\frac{\partial p}{\partial z} = g\rho \dots (3)$$

$$\frac{l}{R \sin \theta} \left[\frac{\partial u}{\partial \lambda} + \frac{\partial(v \sin \theta)}{\partial \theta} \right] + \frac{\partial w}{\partial z} = 0 \dots (4)$$

where

- θ —co-latitude = 90- ϕ , ϕ is the latitude.
- u, v, w —the velocity components along the east(λ), south(θ) and downward (z) directions respectively [LT^{-1}].
- p —hydrostatic pressure [MLT^{-1}].
- ρ —density of sea water [ML^{-3}].
- ρ_o —constant density [ML^{-3}].
- R —radius of the Earth [L].
- l — $2\Omega \cos \theta$ [T^{-1}].
- Ω —angular velocity of Earth's rotation [T^{-1}].
- Au, Av —advective acceleration terms [LT^{-2}].
- F^λ, F^θ —friction terms in the momentum equations [LT^{-2}].
- μ, ν —horizontal and vertical turbulent mixing coefficients respectively [L^2T^{-1}].

$$Af = (Au, Av) = \frac{l}{R \sin \theta} \left[\frac{\partial(uf)}{\partial \lambda} + \nu \frac{\partial(f \sin \theta)}{\partial \theta} \right] + \frac{\partial(wf)}{\partial z}$$

$$F^\lambda = \frac{\partial \left(\nu \frac{\partial u}{\partial z} \right)}{\partial z} + \mu \left[\Delta u - \frac{u}{R^2 \sin^2 \theta} + \frac{2 \cos \theta}{R^2 \sin^2 \theta} \frac{\partial v}{\partial \lambda} \right]$$

$$F^\theta = \frac{\partial \left(\nu \frac{\partial v}{\partial z} \right)}{\partial z} + \mu \left[\Delta v - \frac{v}{R^2 \sin^2 \theta} + \frac{2 \cos \theta}{R^2 \sin^2 \theta} \frac{\partial u}{\partial \lambda} \right]$$

Δ —Laplacian operator

$$\Delta f = (\Delta u, \Delta v) = \frac{l}{R^2 \sin^2 \theta} \frac{\partial^2 f}{\partial \lambda^2} + \frac{l}{R^2 \sin \theta} \frac{\partial \left(\sin \theta \frac{\partial f}{\partial \theta} \right)}{\partial \theta}$$

Boundary conditions

At the ocean surface ($z=0$), the following boundary conditions were applied for the velocity fields.

$$\rho_o \nu \frac{\partial u}{\partial z} = -\tau_\lambda; \rho_o \nu \frac{\partial v}{\partial z} = -\tau_\theta; w|_{z=0} = 0 \dots (5)$$

where τ_λ and τ_θ are the components of wind stress in the zonal and meridional directions respectively and u, v are the components of velocity fields.

At the bottom $z=H(\lambda, \theta)$, non-slip boundary condition for velocity fields was applied.

$$i.e. u=v=w=0 \dots (6)$$

At the rigid lateral boundaries, the normal flux boundary conditions of zero velocity is prescribed.

$$i.e. \vec{v}_n = 0 \dots (7)$$

where 'n' is the normal to the boundary.

There are two open boundaries in the model area; the first zonal open boundary passes through 20°S latitude between the longitudes 35°E and 80°E and the second meridional open boundary passes along the longitude 80°E (Fig.1). At the open sea boundaries, the velocity components computed with the help of a quasi-geostrophic model of Marchuk & Sarkisyan³ were used.

Initial conditions

An initial state of rest is considered for the velocity components u and v before starting the integration.

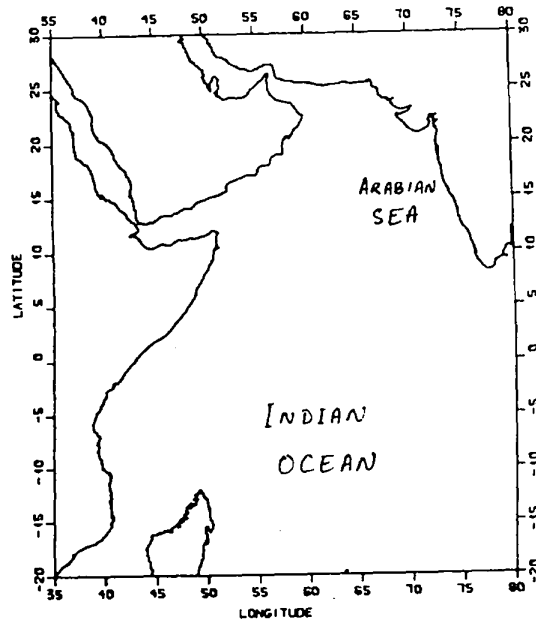


Fig. 1—Location of study.

$$\text{i.e. } (u, v)_{t=0} = 0 \quad \dots (8)$$

The density of sea water ' ρ ' can be expressed as the sum of the average density ' ρ_0 ' and the density anomaly ' $\rho'(\lambda, \theta, z)$ '. The expression for hydrostatic pressure at a depth z can be obtained by integration of the hydrostatic Eq. (3) in the vertical from free surface to depth z .

$$p = \rho_0 g \zeta + g \int_0^z \rho' dz \quad \dots (9)$$

where ' ζ ' is the sea surface topography or sea level. There are five unknown variables (u, v, w, p and ξ) in four equations [Eqs (1)-(4)]. In order to have a closed system of model equations, it requires to have an expression for sea level ξ . The procedure to derive sea level equation is explained in the work of Bahulayan & Shaji².

The Eqs (1)-(4), taking into account the equation for hydrostatic pressure (Eq. 9) are solved with the help of a leap-frog numerical scheme. By summing the equation of continuity along all levels taking into account the boundary condition at the surface and bottom for vertical velocity (i.e. $w=0$), the two-dimensional integral continuity equation which is the equation for sea surface topography at the internal grid points is obtained. By applying the lateral boundary condition for velocity fields and substituting it in the two-dimensional integral continuity equation, the equation for sea surface topography at the boundary points are also obtained. The sea surface topography equation is solved by successive overrelaxation technique.

Numerical experimentation

The solutions are obtained on a 46x51 staggered grid. Model Eqs (1)-(4) considering Eq (5) were solved subject to the boundary and initial conditions mentioned above using a leap-frog numerical scheme. To inhibit time-splitting instability normally encountered in the leap-frog scheme, a Matsuno scheme which averages solution at two consecutive time steps was employed at every 24 time steps. Equations are integrated forward in time with a time step Δt of 1 hour for approximately 30 days to obtain a steady state solution. The horizontal and vertical turbulent viscosity coefficients used in the model are $5 \times 10^8 \text{ cm}^2 \text{ s}^{-1}$ and $10 \text{ cm}^2 \text{ s}^{-1}$ respectively.

The model is driven mainly by the wind stress at the sea surface and thermohaline field at different levels as the forcings. The wind stress and thermohaline forcings are provided from the climatology of Hellerman & Rosenstein⁴ and Levitus⁵ respectively. In the following sections, results of numerical experiments for the winter and spring seasons at the depths 20 and 50 metres are presented.

Results and Discussion

Currents and sea surface topography for the winter season

Spatial distribution of mean resultant wind stress for the winter season is given in Fig.2. During winter, the NE monsoon winds blow as northeasterly and easterly in the Arabian Sea north of the equator. Very weak northwesterly winds prevail north of 22°N latitude. The strength of northeasterly winds are very high off the Somali region, and after crossing the equator its strength is reduced. The SE trades in the Southern Hemisphere ranges between 10°S and 20°S latitude.

The presentation of σ_t fields seems most appropriate to explain the steady state circulation

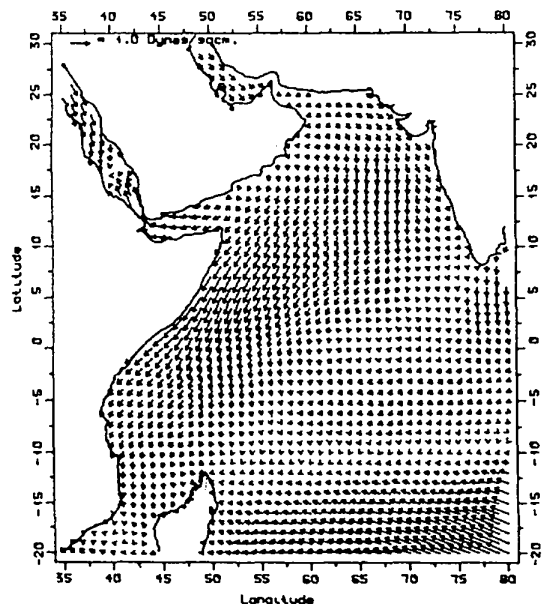


Fig. 2—Spatial distribution of resultant wind stress (dynes·cm⁻²) during winter season

in response to the constant and local forcings of wind stress and density variation. Accordingly, the σ_t fields at 20 and 50 metres depths are presented in Fig. 3. In both the depths, high dense water is found in the northern and central Arabian Sea. The presence of high dense waters in these regions can be attributed to the excess of evaporation and the penetration of high saline Persian Gulf and Red Sea waters into the northern and central Arabian Sea. σ_t fields decreases gradually from north to south in both the depths. There is very sharp density gradient off the southwest coast of India and the same is caused by the advection of low saline Bay of Bengal waters towards this region.

The model computed currents and sea surface topography are shown in Figs 4 and 5 respectively. The surface circulation at 20 m depth (Fig. 4a) shows that Arabian Sea north of the equator is covered by NE monsoon current which mainly flows westward and southwestward, and is a resultant of prevailing winds and thermohaline forcing. There is a weak southwestward flow north of 20°N. The westward flowing North Equatorial Current (NEC) observed between 5°N and 10°N branches into two off the Somali region; one flows north of 5°N as a northward flow and the other south of 5°N as the southward Somali

Current (SC). The South Equatorial Current (SEC) ranges between 20°S and 10°S in the Southern Hemisphere. The model Equatorial Counter Current (ECC) is found in the Southern Hemisphere between 8°S and 3°S east of 45°E, fed jointly by the SEC and southward SC. The model computed surface currents such as the westward NEC and SEC, southward SC and eastward ECC is in good agreement with the ship drift measurements of surface currents compiled by Cutler & Swallow⁶.

The model computed sea surface topography (Fig.5) shows a zonally oriented ridge with steep equatorward downward slope south of 20°S latitude. This ridge region, in fact, represents the domain of SEC which does not vary much during different seasons. Along the east African coast, the sea level is high and hence the flow is offshore. Sea level is high off the southwest coast of India, which causes a northward flow in this region.

The computed circulation at 50 m depth (Fig.4b) shows that flow field has changed north of 10°N compared to 20 m depth, and a weak cyclonic circulation is observed in this region. The southward SC is still persisting, but weakened compared to 20 m depth. A weak Equatorial Under Current (EUC) is also observed between 2.5°S and

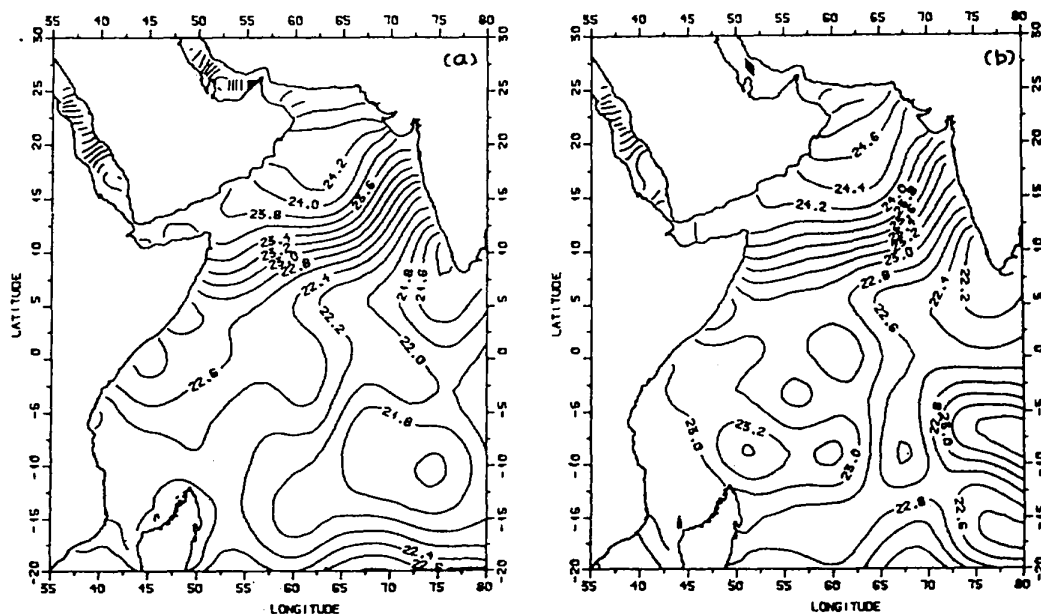


Fig. 3—Spatial distribution of σ_t during winter at (a) 20 m depth (b) 50 m depth

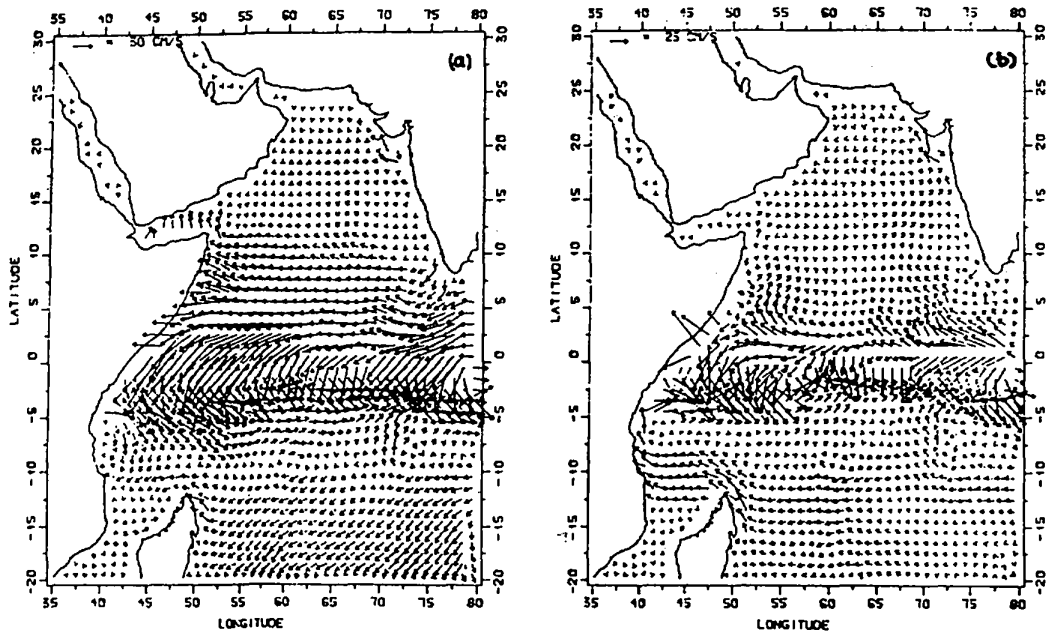


Fig. 4—Computed current (cm sec^{-1}) during winter season at (a) 20 m depth (b) 50 m depth

7.5°S latitude. SEC, between 10°S and 20°S latitude, has become more zonal. This orientation is mainly due to the presence of thickly packed sea level contours in this region.

Currents and sea surface topography for the spring season

The wind field is southerly and southeasterly in the entire Southern Hemisphere and it turns southwesterly and westerly on approaching the equator (Fig. 6). Southwesterly and westerly winds with magnitudes up to $1.5 \text{ dynes cm}^{-2}$ are found in the entire Arabian Sea. In the equatorial belt between 2.5°N and 2.5°S, the strength of wind stress east of 60°E is very less.

The σ_t fields at 20 m and 50 m depths are depicted in Fig. 7. During the premonsoon season, upwelling begins off the coasts of Somali and Arabia, the surface layer is cooled and hence high dense water can be seen off the coasts of Arabia, Somali and Africa at 20 m and 50 m depths. The temperature gradually increases towards east and hence low dense water is observed off the southwest coast of India and central equatorial Indian Ocean.

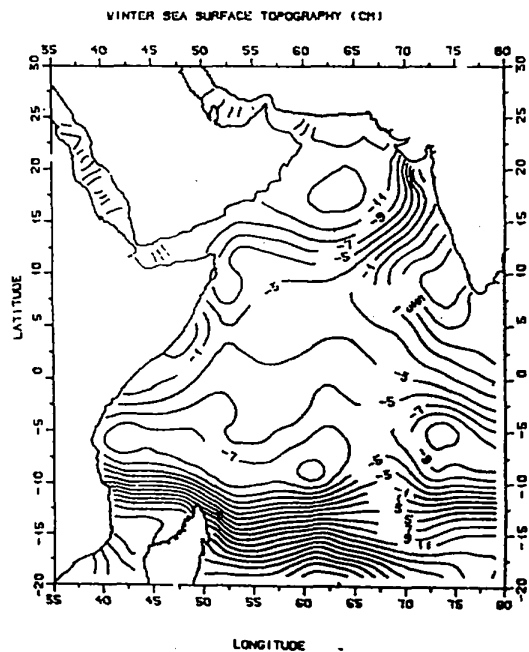


Fig. 5—Computed sea surface topography (cm) during winter season

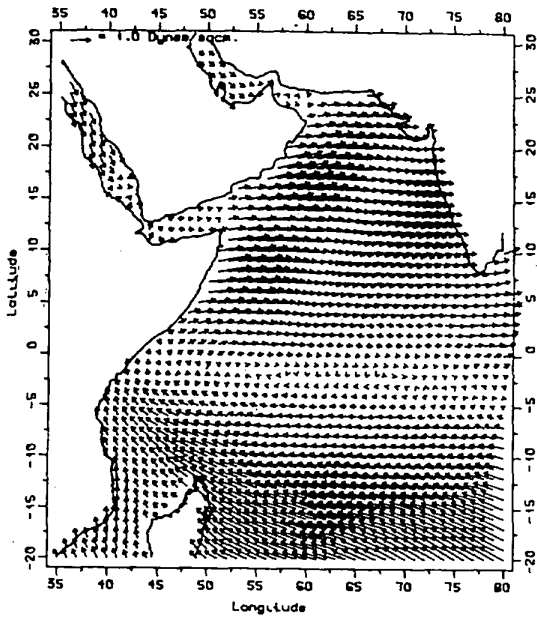


Fig. 6—Spatial distribution of resultant wind stress (dynes·cm⁻²) during spring season.

Figure 8 shows the computed currents at 20 m and 50 m depths whereas Fig. 9 shows the computed sea level. Surface current regime at 20 m depth shows the presence of broad SEC between 10°S and 20°S latitude. Thickly packed zonally oriented sea surface topography contours in the Southern Hemisphere also reflect the presence of SEC in the model area. Another interesting feature of computed currents during spring is the presence of eastward Equatorial Jet (EJ) between 2°N and 2.5°S, east of 50°E longitude. Occurrence of EJ in the tropical Indian Ocean during the spring season has been reported first by Wyrki⁷ & Molinari *et al.*⁸ also observed the same in the monthly climatology of surface currents using surface drifting buoy data. The northern Arabian Sea is mainly covered by southeastward flow with a maximum velocity of 50 cm sec⁻¹. The sea surface topography contours (Fig.9) show high sea level off the southwest coast of India due to the presence of low dense water in this region and hence a weak northward flow is expected. However, the computed flow is southeastward which is caused by the westerly winds in this region dominating the effect of sea

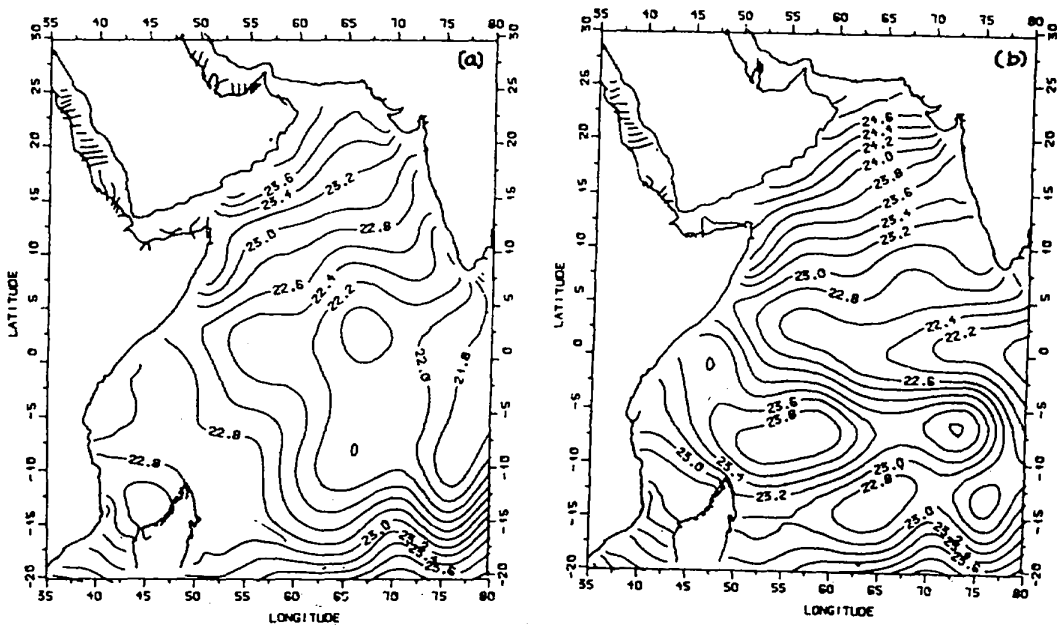


Fig. 7—Spatial distribution of σ_t during spring at (a) 20 m depth (b) 50 m depth

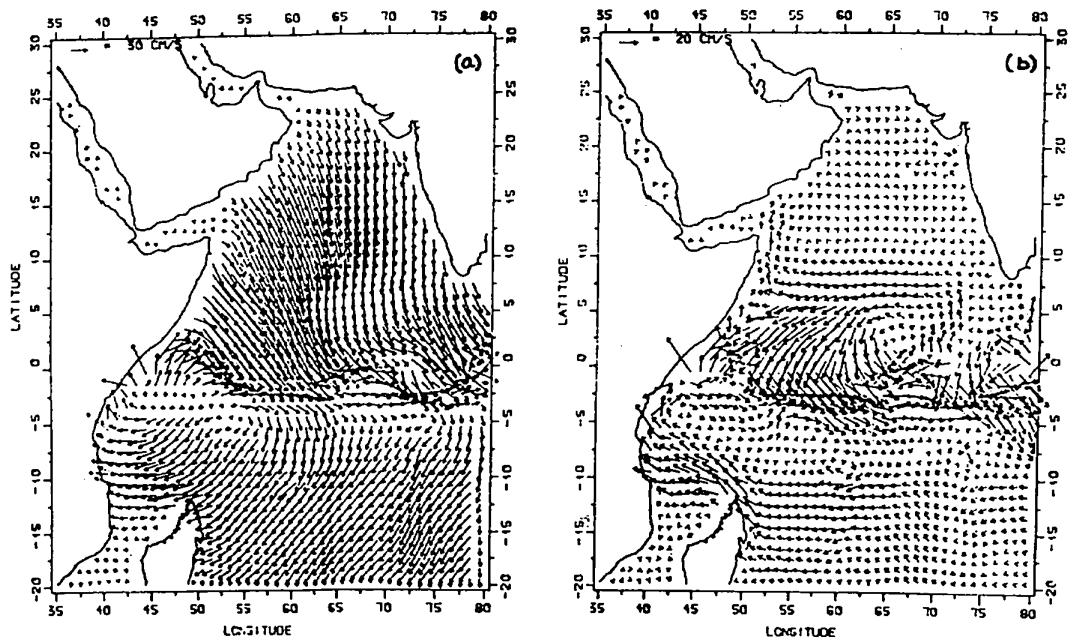


Fig. 8—Computed current (cm sec^{-1}) during spring season at (a) 20 m depth (b) 50 m depth.

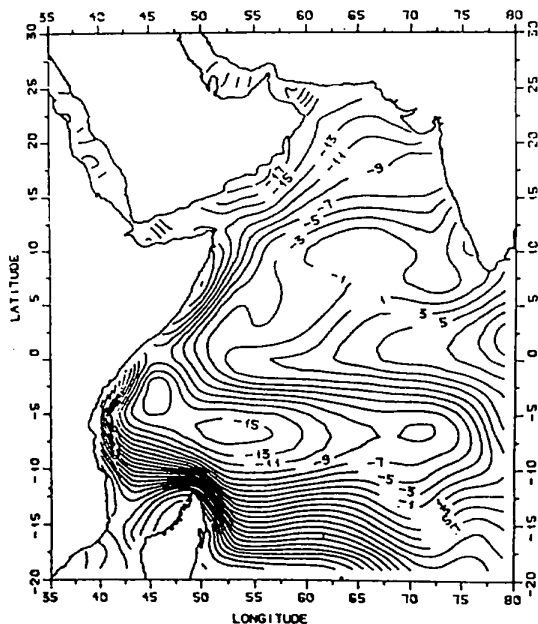


Fig. 9—Computed sea surface topography (cm) during spring season.

level and baroclinic forcing. The currents off the Africa and southern Somalia show northward component, which is the real situation during premonsoon season. A big cyclonic gyre is formed off the African coasts between 10°S and 4°N latitude. Model results show all the major features such as the SEC, EJ, cyclonic gyre off the African coast, southeastward flow off the west coast of India at the surface level. These features can also be seen in the ship drift currents of Cutler & Swallow⁶.

The SEC and EJ computed at 20 m depth is found at 50 m depth also (Fig. 8b), otherwise the circulation pattern at 50 m depth is different from the one at 20 m. The intensity of SEC is diminished at 50 m, and EJ is shifted more towards the south between 2.5°S and 5°S , east of 55°E longitude. There is a westward flow between the southwest coast of India and northern Somali. The flow, in general, is northward all along the coasts of Africa and Somali. The flow off the southwest coast of India shows a weak northward component. This can be interpreted as to the presence of high

sea level in this region, which generates a northward geostrophic flow at subsurface level.

Acknowledgement

Authors are grateful to the Head, Centre for Atmospheric Sciences, IIT, New Delhi and Head, Data Division, NIO, Goa for providing necessary facilities. One of the authors (C.Shaji) is indebted to the Council of Scientific & Industrial Research, New Delhi for financial assistance.

References

- 1 Gill A E, *Atmosphere-Ocean Dynamics*, (Academic Press, New York) 1982, pp. 662.
- 2 Bahulayan N & Shaji C, *Proc Indian Nat Sci Acad (Physical Sciences)*, 62A (1996) 325.
- 3 Marchuk G I & Sarkisyan A S, *Mathematical modelling of ocean circulation*, (Springer-Verlag, Berlin), 1988, 292.
- 4 Hellerman S & Rosenstein M, *J Phys Oceanogr*, 13,7 (1983), 1093.
- 5 Levitus S, *Climatological Atlas of the world ocean*, NOAA prof. paper 13 (US Government Printing Office, Washington D C), 1982, pp. 173.
- 6 Cutler A N & Swallow J C, *Surface currents of the Indian Ocean* (Institute of Oceanographic Sciences, U K), 1984, pp. 8.
- 7 Wyrtki K, *Oceanographic Atlas of the International Indian Ocean Expedition* (NSF, Washington D C), 1971, pp. 531.
- 8 Molinari R L, Olson D & Reverdin G, *J Geophys Res*, 94, C5 (1990), 7217.